Milling parameter optimization for refinement of NiO/Al mixtures and synthesis of Ni/Al_2O_3 nanocomposites.

N.E.H. Berramdan [a], H. Boutefnouchet [b], M. Zidani [c, d], R. Yamanoglu [e], C. Curfs [f]

[a] *Laboratory of Mining, Metallurgy and Materials (L3M), National school of mining and metallurgy (ENSMM) Amar Laskri, Annaba, 23000, Algeria.*
[b] *Laboratory of Foundry research (LRF), University of Badji Mokhtar, Annaba, 23000, Algeria.*
[c] *Laboratory of Energy Engineering and Materials (LGEM), University of Mohamed Khider, Biskra, 07000, Algeria.*
[d] *Faculty of technology, University of Batna 2, Batna, 05000, Algeria.*
[e] *Department of metallurgy and materials engineering, University of Kocaeli, Kocaeli, 41001, Turkey.*
[f] *European Spallation Source ERIC, P.O. Box 176, SE-221 00 Lund, Sweden.*

Corresponding author e-mail address: nor-el-houda.berramdane@ensmm-annaba.dz

(Received 30 September 2023; Accepted 22 January 2024)

Abstract

This study examined the effect of milling parameters on the development of Ni/Al_2O_3 nanocomposites and refinement of NiO and Al powders. Ball milling of certain mixtures was followed by sintering at 800 and 1100 °C for 2 h. The X-ray diffraction results of the dry-milled powders indicated that increasing the ball-to-powder weight ratio from 20:1 to 42:1 produced finer particles, resulting in the synthesis of Ni/Al_2O_3 nanocomposites by milling at 200 rpm for 1.5 h. Extending the milling duration at lower rotational speeds yielded powders with nanoscale particle sizes. However, as observed under scanning electron microscopy and energy dispersive spectroscopy, a metallic matrix nanocomposite was formed *via* the mechanochemical reaction, and the crystallite size was estimated using the Williamson–Hall plot. Furthermore, using differential scanning calorimetry plots, we analysed the effect of milling on the temperatures of phase transformation and/or reduction reactions. The tribological performance of the developed nickel metal matrix composite was examined by employing a ball-on-disc tribometer at various load conditions. Indeed, the friction coefficient increases with applied forces and decreases with milling. Comprehensive examinations of the worn surfaces were conducted through the utilization of a scanning electron microscope and a 3D optical profiler.

Keywords: Mechanical alloying, Ni/Al_2O_3 nanocomposite, Sintering, Aluminothermic reduction, Friction coefficient, Wear mechanism.

1. Introduction

The mechanical alloying (MA) technique is widely employed to synthesise new nanocomposite materials for a variety of applications. Mechanochemical reactions are defined as chemical reactions (exchange reaction, reduction/oxidation, decomposition of compounds, or phase transformation) occurring during the milling process. Among these reactions, the aluminothermic reaction (thermite reaction) occurs between a metal oxide (NiO, CuO, ZnO, TiO_2, Fe_3O_4, ZrO_2, etc.) and aluminium [1–8]. However, two distinct reaction kinetics can emerge depending on the applied milling parameters: first, a gradual transformation; second, self-propagating high-temperature synthesis (SHS) [9] or combustion synthesis. In principle, the SHS requires a critical period before the ignition is triggered inside the vials during milling. After the gradual increase in the temperature of the vials in the first stage of milling, the temperature increases rapidly, which indicates the ignition of the reaction [10]. In recent years, several

JMMB accepted manuscript

researchers have employed various methods to utilise the NiO/Al system for developing Ni matrix composites incorporating Al_2O_3 particles, which are promising options for applications requiring enhanced wear and corrosion resistance [11-12] . However, Vrel et al. [13, 14] investigated the reaction between NiO and Al *via* SHS by adding various concentrations of alumina and adjusting the stoichiometric ratio of the reagents to minimise the amount of heat released during the thermite reaction, which successfully minimised the sputtering and destruction of the sample. Troncy et al. [15, 16] employed pre-oxidised Ni and Al to fabricate self-regenerating coatings of $NiAl/Al_2O_3$ *via* heat treatment. In addition, high-energy ball milling has been applied to create similar composite materials composed of Al, NiO, and Ni particles. Prior research reported that a critical period of 110 min is required before the ignition of the mixture inside the vials. After 10 h of milling, only the product phases were detected, and upon extending the milling duration to 60 h, refined grain sizes of NiAl and Al_2O_3, *i.e.*, 8-nm particles, were observed [17]. Moreover, NiO/Al powders have been used with other materials to prepare composites with various reinforcements [18–21]. Matteazzi et al [22] employed two types of mill, specifically a vibratory ball-mill and a planetary ball mill, in their study of various M_xO_y and Al systems. The α-Al_2O_3-Ni composite was successfully synthesized within a milling time of 1.5 hours, using a ball-to-powder ratio (BPR) of 42:1. Nevertheless, the literature available on this system is relatively sparse and provides only limited information [22, 27]. Li [23] and Udhayabanu et al. [24] used a ball-to-powder weight ratio (BPR) of 10:1 along with various process control agents to develop Ni/Al_2O_3 nanocomposites from NiO and Al powders, obtaining Ni and amorphous Al_2O_3 after a long periods of milling 10 and 5 h, respectively. They concluded that mechanical activation poses a gradual effect on the reduction of NiO by Al. The synthesis of Ni/Al_2O_3 composite by powder metallurgy process involves (milling and pressure-assisted sintering.) was studied by Mameri et al [25] additionally, they explored the tribological characteristics of these composites as part of their investigation.

According to the literature review, all existing research focusing on the NiO/Al system applied mechanical alloying with various milling However, no study has attempted to optimise the milling conditions, either for refining only the particle size of the reactants or producing Ni/Al_2O_3 nanocomposites. Furthermore, this gap extends to the realm of tribology as well. There has been no investigation into the tribological behavior of Ni/Al_2O_3 composites obtained through the conventional powder metallurgy process, which involves milling, compacting, and sintering. Therefore, the fundamental objective of this study is to display the effect of various milling parameters, *e.g.*, BPR, milling duration, and milling speed on the refinement of NiO/Al powders. Moreover, we attempted to achieve the smallest ignition period required to produce Ni/Al_2O_3 nanocomposite without using any reducing or protective agent under air. We performed sintering tests to validate the results obtained under the adopted milling conditions. Furthermore, we delved into the tribological attributes of the obtained composites and analysed how milling and applied loads affect the friction coefficient and the characteristics of the worn surfaces.

2. Experimental

Aluminium (Al) powder and nickel oxide (NiO) with an average particle size of 74 μm and <44 μm were purchased from Sigma-Aldrich and Acros-Organics, respectively. The powders were weighed with a stoichiometric composition corresponding to the following equation:

$$3NiO + 2Al = 3Ni + Al_2O_3 \quad (1)$$

JMMP accepted manuscript

The mechanical alloying of the powders was conducted using a planetary micromilling Pluverisette 7 premium line FRITISH. Stainless steel vials with a capacity of 80 mL and balls of diameter ∅ = 10 mm were used. Two ball-to-powder weight ratio (BPR) of 20:1 and 42:1, were used with a powder mixture of about 2g and 1g, respectively. Notably, the mechanical alloying was conducted under air and without adding a process-controlling agent (PCA). The milling conditions applied in this study are summarised in the following table.

case	BPR	Speed (rpm)	Time (h)
A	20 :1	100, 150,200 and 250	1
B	42 :1	100,150, 200 and 250	1
C	42 :1	100	1, 2, 3, 4, 5, 8.
D	42 :1	100, 150 and 200	1.5

Table 1. The milling conditions applied to the mixtures of NiO/Al powders.

Prior to initiation, the mill was set up to halt for 15 min after every 30 min of operation; 2 g of the milled powders were uniaxially pressed at room temperature *via* a cylindrical tungsten carbide die (D = 13 mm) under a pressure of 510 MPa. Subsequently, the compacted samples were subjected to sintering using a tubular electric furnace in a neutral atmosphere provided by a vacuum pump at 800 and 1100 °C. In addition, differential scanning calorimetry (DSC) was performed for the green mixture, and an amount of the milled powders was heated at a rate of 25 °C/min in an argon atmosphere using a Netzsch STA 449 F3 Jupiter® to determine the thermal stability of the various samples. The particle morphology evolution of the milled powders and sintered samples was analysed using a Philips XL30 and FEI Quanta-250 scanning electron microscopes (SEM) equipped with an energy dispersive X-ray spectrometer (EDS). The structural evolution and phase formation occurring during mechanical alloying was determined using high-resolution powder X-ray diffraction (HRPXRD) performed at the ID 31 beamline (E_i = 31 KeV, corresponding to λ = 0.4 Å) of the European Synchrotron Radiation Facility (ESRF) in Grenoble and X-ray diffraction (XRD, X-Pert Panalytical) using Cu–Kα radiation for the sintered samples. Furthermore, the Williamson–Hall plot (W–H) method was used to calculate the crystallite size and lattice strain of the milled samples [26]. The tribological characteristics were evaluated by employing a ball-on-disc tribometer (CSM tribometer, manufactured by CSM Instruments Inc., located in Peseux, Switzerland) with alumina balls (diameter= 6mm) as a counter-face material. The measure of volume loss on the worn surface was acquired through the utilization of CT 100 a 3D optical profilometer.

3. Results and Discussion

3.1. *Milling process*

3.1.1. X-Ray Diffraction

Effect of the ball to powder weight ratio (BPR)

The XRD plots of the specimens milled for 1 h as a function of milling speed (100, 150, 200, and 250 rpm) with a BPR of 20:1 representing Case A and a BPR of 42:1, representing Case B in Table 1 are depicted in Figures 1 and 2. As observed, the as-received powder mixture was characterised by sharp intense peaks, reflecting the higher crystallinity of NiO and Al powders. However, as the milling speed increased up to 200 rpm, the NiO and Al peak intensities notably diminished with large broadening of the peaks, which was potentially caused by the gradual reduction in the crystallite size of the reactants coupled with the increased lattice strain during milling. Furthermore, milling with a rotation speed of 250 rpm generated Ni and Al_2O_3 particles, indicating

MMB_accepted_manuscript

that the aluminothermic reaction between NiO and Al occurred during the mechanical alloying process (Eq. 1) by a self-propagating reaction as noted earlier [23]. However, as observed from Figures 1 and 2, the peaks ascribed to the NiO phase are still present when the thermite reaction took place, suggesting oxidation of a small amount of nickel after reaction and during cooling, due to the processing conditions in air. Notably, as the BPR increased to 42:1 the peak attributed to the nickel particles broadened, indicating that alumina became sharper; however, their peaks broadened wider than those of Ni and Al_2O_3 obtained in the first case with a BPR of 20:1.

The crystallite size of the green mixture particles was 491 nm for NiO and 810 nm for Al. As such, milling at a speed of 200 rpm and BPR of 20:1 produced NiO and Al particles with a diameter of 79.7 and 325 nm, respectively. However, the grain sizes of the NiO and Al particles obtained with a BPR of 42:1 were 64.5 and 212 nm, respectively. Moreover, the grain sizes of Ni and Al_2O_3 of case B were 87 and 78 nm with a lattice strain of 0.171 and 0.241%, respectively (Table 2). As the particle size of the reinforcement (Al_2O_3) and metallic matrix (Ni) were less than 100 nm, the results confirmed the formation of a nanocomposites [27]. Milling cannot reduce Al particles to an extremely fine crystallite size owing to its ductility [17]. As fresh surfaces were generated by the reduction of the crystallite size *via* repeated cold welding and fracturing, the reactions that require elevated temperatures were rendered feasible at low temperatures [28]. During the phase transformation, the temperature of the vials increased, which can be attributed to the highly exothermic reaction between NiO and Al powder, exceeding 3156 K [29-30]. Prior to milling, the mixed powders were pale green in color, which subsequently varied to two distinct colours: first, a dark-green color for samples with no thermite reaction during mechanical alloying (100, 150, and 200 rpm); second, a black color related to the reduction of the NiO by Al into a Ni/Al_2O_3 nanocomposite (250 rpm), which are consistent with the previously reported observations [31].

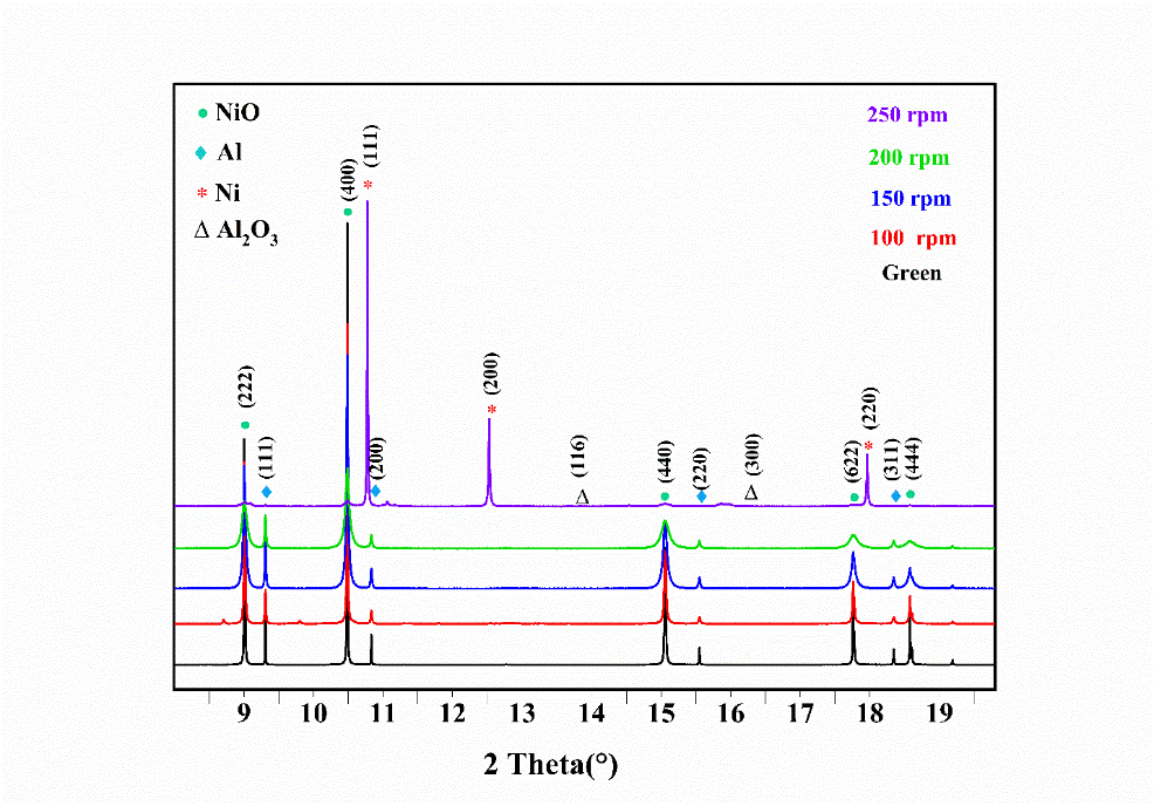

Figure 1. XRD plots of pure and milled NiO/Al powder mixture with a BPR of 20:1 milled for 1 hour as a function of milling speed 100,150,200 and 250 rpm.

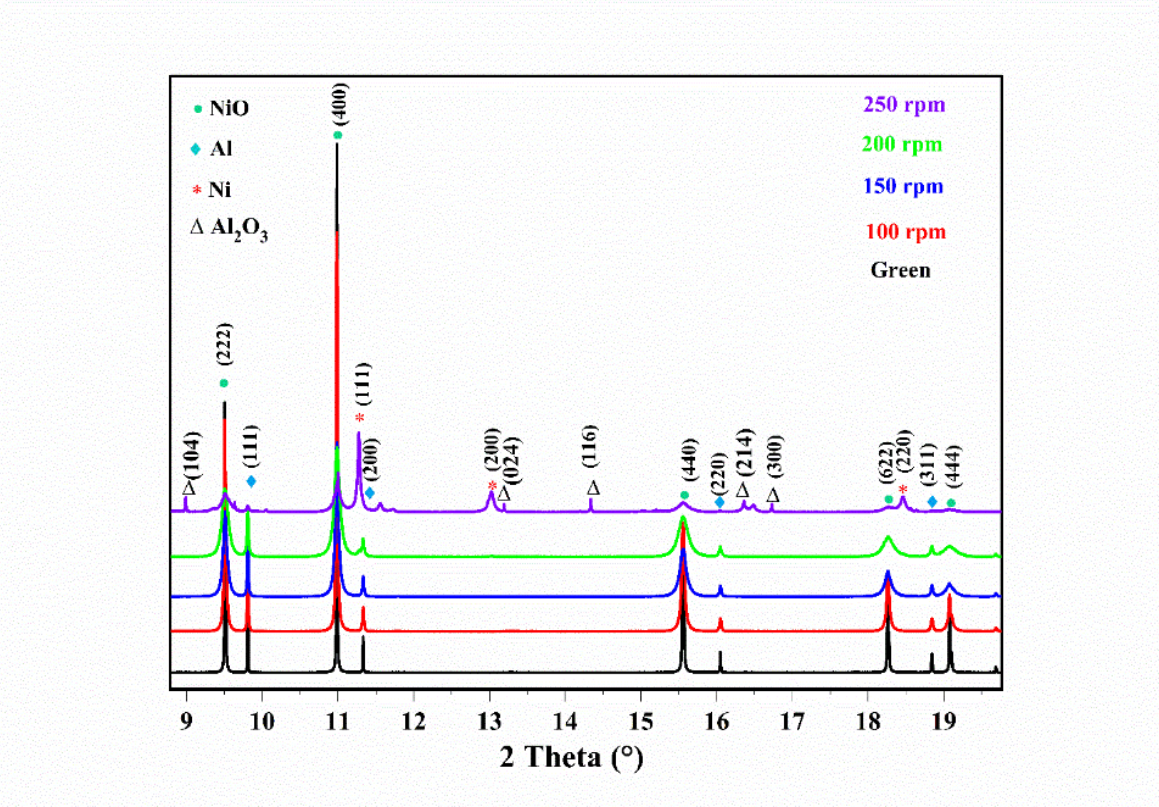

Figure 2. XRD plots of specimens milled for 1 hour as a function of milling speed (100,150,200 and 250 rpm) with a BPR of 42:1.

BPR	Speed (rpm)	D NiO (nm)	D Al (nm)
20:1	100	497	800
	150	113	366
	200	79.7	325
	250	D Ni (nm)	DAl2O3 (nm)
		564	144
42:1	100	206	759
	150	83	316
	200	64.5	212
	250	D Ni (nm)	DAl2O3 (nm)
		87.8	78

Table 2. Mean crystallite size of NiO, Al, Ni and Al_2O_3 after milling for 1h as a function of milling speed for a BPR of 20:1 and 42:1.

Effect of milling duration.

Based on the first two cases, we concluded that increasing the BPR to 42:1 yields finer particles. Therefore, pure and milled NiO/Al powders blended for various milling periods (1, 2, 3, 4, 5, and 8 h) with a BPR of 42:1 and rotation speed of 100 rpm are visualized in Figure 3, representing Case C in Table 1. As observed, no additional peaks were detected corresponding to any other new

JMMB_acer

or intermediate phases, and both NiO and Al peaks continued to exist. However, milling up to 8 h with a small rotation speed did not alter the composition of the product. The broadness of the NiO and Al peaks increased significantly with the milling duration. Moreover, the prolonged milling duration aided the development of homogenous powders at a nanometre scale, which can be attributed to the equilibrium achieved between the mechanisms of fracturing and cold welding [1]. Furthermore, the ball milling process can impact the crystallite size by inducing dislocations during the formation of sub-grains[32].

The crystallite size and lattice strain evolution are presented in Figure 4 as a function of milling period determined using the W–H plot method. According to the data acquired from the NiO peaks, the mean particle size after milling for 1 h was observed to be approximately 206 nm. Upon milling for 3 h, the crystallite size decreased considerably to 104 nm, and after milling for 8 h, the particle size further decreased to 76.2 nm. However, as per the W-H relation, the lattice strain should be inversely proportional to the crystallite size, which is not exactly the case in our analysis. It is proportional up to 3 h, after that the crystallite size is stabilized while the lattice strain is increased. A possible explanation for this phenomenon is the increase of stacking fault energy during milling, which impede the formation of new crystallite and increase the strains due to impacts during milling [33, 34].

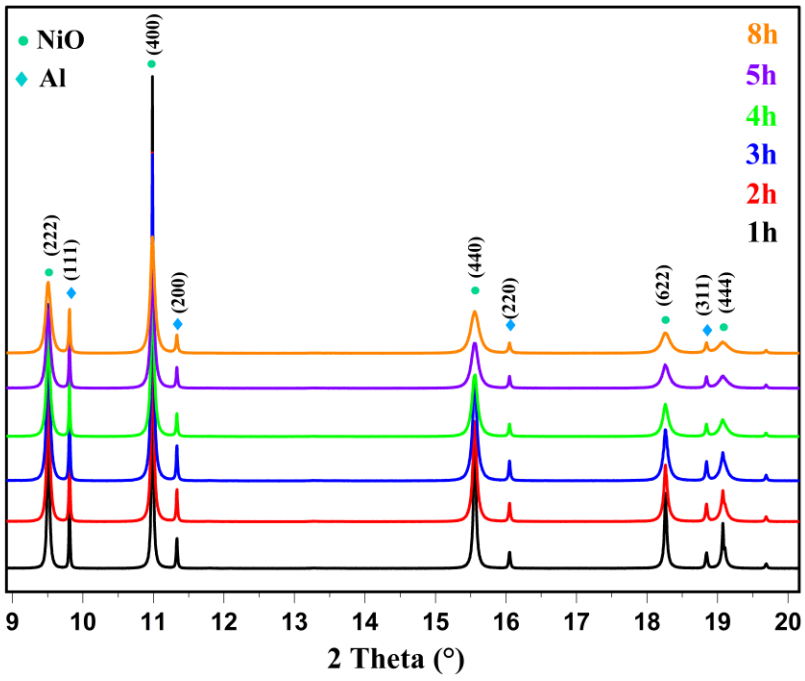

Figure 3. XRD plots of pure and milled NiO/Al powders blended for different periods of milling time 1, 2, 3, 4, 5 and 8h with a BPR of 42:1 and a rotation speed of 100 rpm.

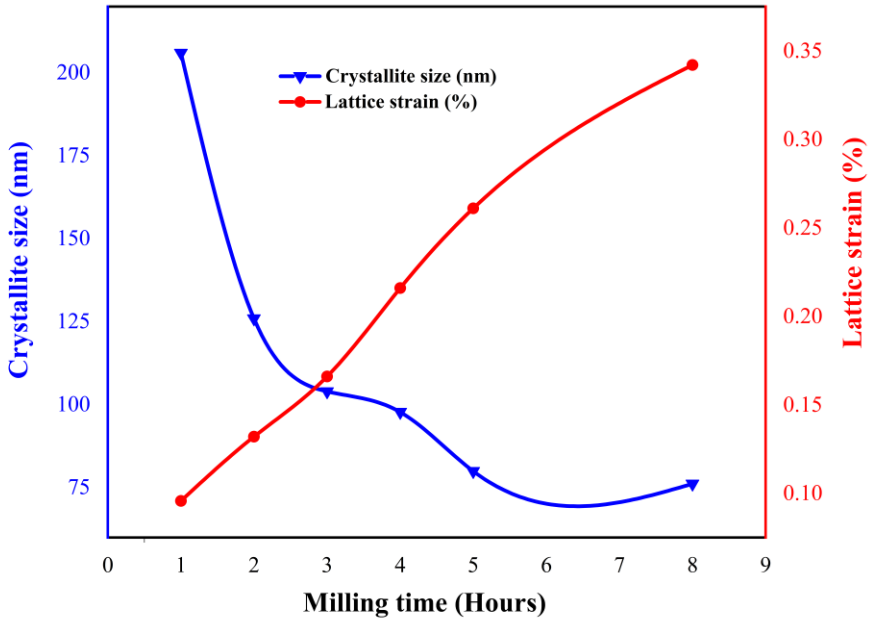

Figure 4. The crystallite size and lattice strain evolution as a function of milling time.

Effect of milling speed

The XRD patterns of pure and milled powders for 1.5 h using a BPR of 42:1 for varying milling speeds of 100, 150, and 200 rpm are illustrated in Figure 5. In Case D, the Ni/Al_2O_3 nanocomposite was formed only upon applying a milling speed of 200 rpm. This result is consistent with the literature on the same system[22, 27]. Milling with a speed of 100 and 150 rpm only activated the powder mixture and refined the reactant particles. The mechanical activation of the powders during milling can be related to the repeated collusion applied to the particles between the balls and vial walls or between the balls [35]. The objective of searching for optimal conditions to enhance the refinement of NiO/Al powders is to generate mechanically activated and finely refined powders. The milling time is a key factor in the milling process and is closely related to the Ball-to-Powder Ratio (BPR) [27]. A larger BPR results in higher milling intensity and a shorter time required for reaction completion, and vice versa. The selection of BPR in this study was determined based on relevant literature[22], [27]. Prolonged milling time increases the risk of contamination and the formation of undesirable phases[27]. It also necessitates the use of a diluent[22], and excessively high speeds can strongly accelerate the reaction without achieving the desired refinement of the co-milled powders. These refined powders will then be introduced into the Ti-C system to assess their impact on the ensuing TiC synthesis reaction, as part of an upcoming study. Notably, in all Cases (A, B, C, and D), the intensity of the peaks ascribed to Al was substantially less than that of NiO owing to the low volume fraction of Al in the primary mixture (80.6 wt.% of NiO with 19.4 wt.% of Al). The disappearance of the Al_2O_3 peaks in this sample was possibly caused by the low volume fraction of the new phase formed during milling, which is related to the extremely fine particles obtained. Moreover, as NiO is extremely brittle in nature, it reduces to ultrafine sizes after milling. The crystallite sizes of the Ni and Al_2O_3 phases determined using the W–H plot method were 85 and 45 nm, respectively. As reported by

Suryanarayana, the evolution of the grain size depends on increasing the milling energy and BPR at low temperatures [1].

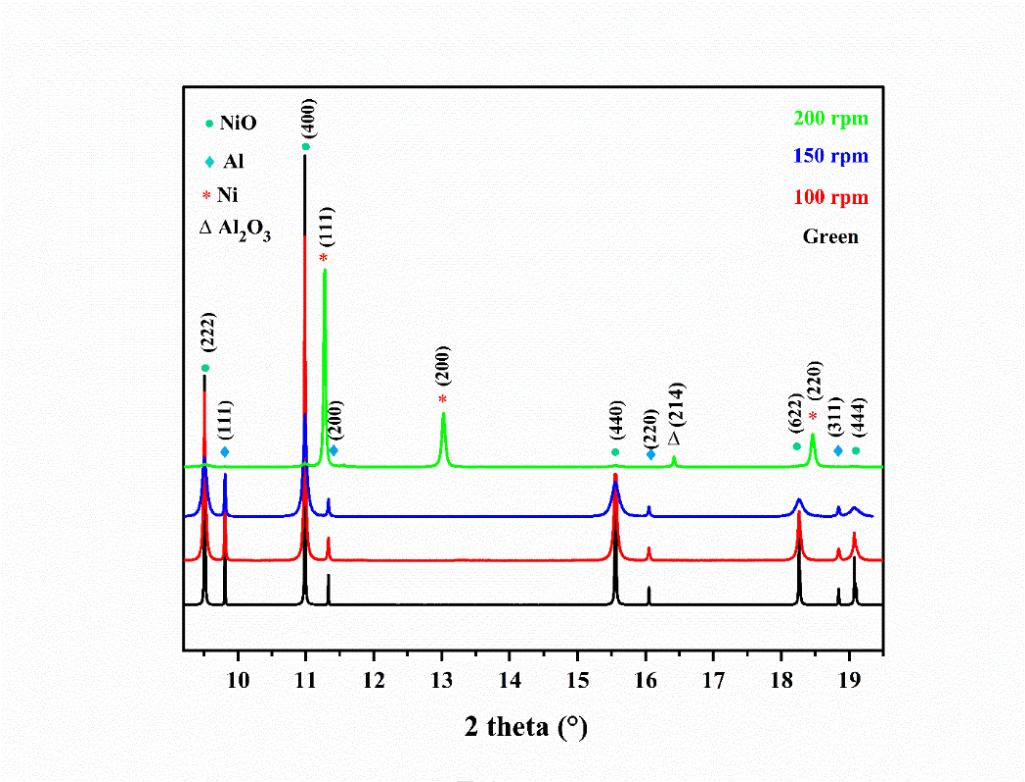

Figure 5. XRD patterns of pure and milled powders during 1.5 hour using a BPR of 42:1 for different milling speed 100,150 and 200 rpm.

3.1.2. SEM Microstructure

The SEM micrographs of the unmilled and milled samples for 1 h at 200 rpm are depicted in Figure 6 for BPR 20:1 and 42:1. As observed, the unmilled powder mixture exhibited a particle morphology composed of irregular particles of Al surrounded by smaller grains of NiO. The size of the Al and NiO particles diminished significantly upon milling. The inhomogeneous distribution of these particles produced an irregular morphology. Moreover, the fine particles were agglomerated by the repeated fragmentation and cold welding of the powders due to the absence of a process control agent (PCA). The PCA in the mixture ensured that the particle surfaces do not face any barrier between themselves or against the vials [1]. Moreover, the SEM images of the samples displaying the presence of Ni and Al_2O_3 phases in their XRD spectra because of the mechanochemical reaction at the end of the milling process are presented in Figure 7. Two phases, bright and dark, corresponding to the Ni and Al_2O_3 phases, respectively, were observed with small irregular particles and a few agglomerates, but with finer product particles. Thereafter, a specimen milled with a BPR of 42:1 and 250 rpm for 1 h (Figure 7(d)) revealed another morphology. The refinement of the product grains was evident, indicating the predominant fracture in the cold-welding process following the reduction reaction. This result is consistent with previous reports on similar systems [36, 37] as confirmed from the EDS analyses (Figure 7(e–f)). For a BPR of 20:1 and speed of 250 rpm for 1 h (Figure 7(a)), the average size of the Ni particles ranged from

500 to 700 nm (Figure 7(b)), which confirms the previous reports of Ni particle size calculated using the W–H plot method. Moreover, the same observations are recorded in Figure 7(c).

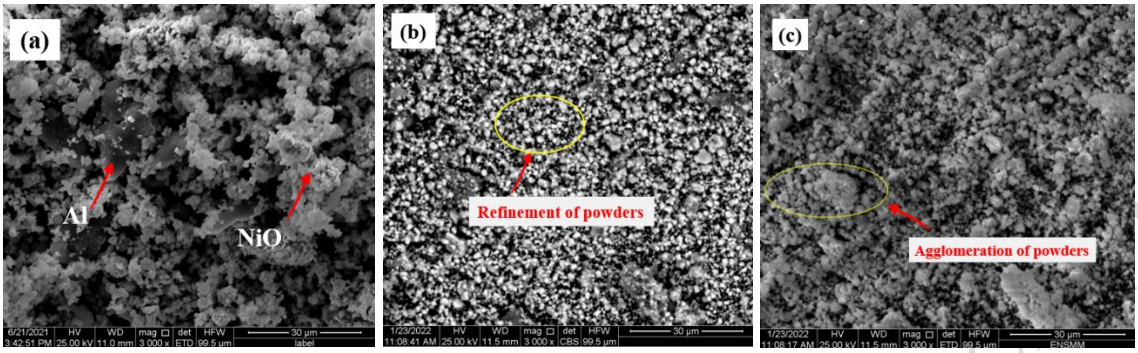

Figure 6. SEM micrographs of unmilled and milled samples with a rotation speed of 200 rpm for 1hour (a) unmilled (b) BPR 20:1 (c) BPR 42:1.

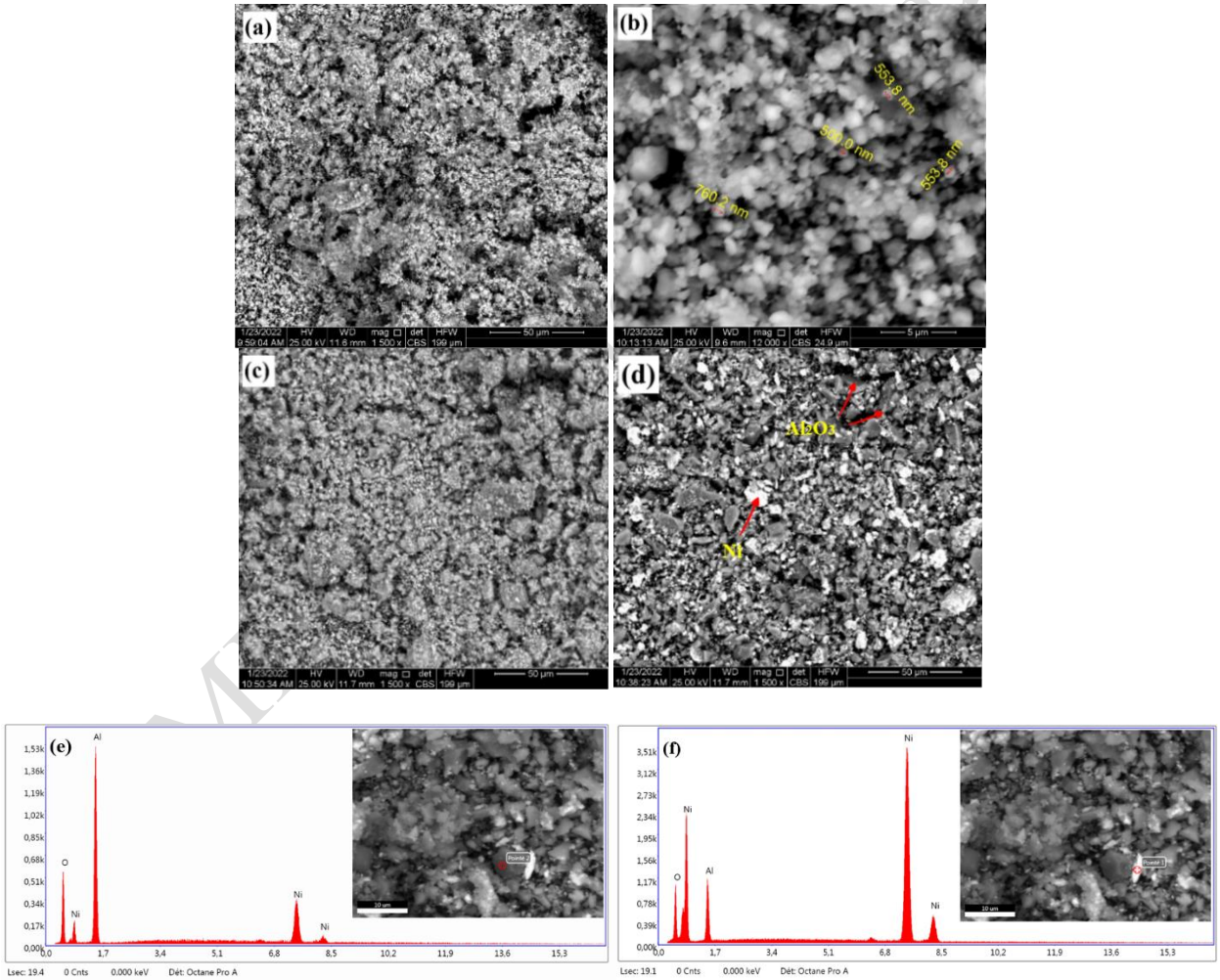

Figure 7. SEM micrographs and EDS plots of samples (a, b) milled with BPR of 20:1 and 250 rpm for 1 hour, (c) BPR of 42:1 and 200 rpm for1.5 hour, (d) BPR of 42:1 and 250 rpm for 1 hour, (e, f) EDS of sample d.

3.1.3. Differential Scanning Calorimetry analysis DSC

To further explain and understand the kinetics of the thermite reaction, a range of samples correlated with the previous results of the XRD analysis were treated using DSC. The DSC profile of the unmilled NiO/Al powder mixture heated at a rate of 25 °C min^{-1} is plotted in Figure 8. The first endothermic peak was observed at 665 °C, corresponding to the melting temperature of Al, whereas the exothermic peak detected at 1015 °C represents the NiO reduction according to Equation (1). This result confirms that the reaction between NiO and Al occurs at a high temperature after the melting of Al, which is consistent with the findings of Udhayabanu [24] and Padhan [31]. DSC curves of mechanically activated samples were identical to those of the unmilled sample, varying only in terms of the onset temperature. The sample milled with a BPR of 20:1 and rotation speed of 250 rpm for 1 h is similar in shape and nature to the sample milled with a BPR of 42:1 and speed of 200 rpm for 1.5 h. However, the two exothermic peaks observed at 454 and 591 °C are likely to be associated with the partial reduction of NiO. Notably, a small endothermic peak was observed at 636 °C, which was certainly related to the melting temperature of Al. The ultimate exothermic peak observed at 910 °C was related to the exothermic reaction between the unreacted NiO and melted Al, which resulted in the formation of the Ni/Al_2O_3 nanocomposite. The DSC curve of the sample milled with a BPR of 42:1 at 250 rpm for 1 h exhibited a distinct pattern, displaying a faint exothermic peak at 982 °C that represents the complete reduction of NiO. The absence of the Al endothermic peak indicated that the entire Al was oxidised in the mixture. More importantly, the benefit of mechanical alloying on powders where a thermite reaction can occur results in a lower ignition temperature for the combustion synthesis [4]. No endothermic peak corresponding to the melting of NiO was observed in any of the DSC curves due to its exceptionally high melting temperature of 1984°C, which is above the temperature range covered by the DSC analysis. These results are consistent with the XRD patterns of the sintered samples.

JMMB _accepted_manuscript

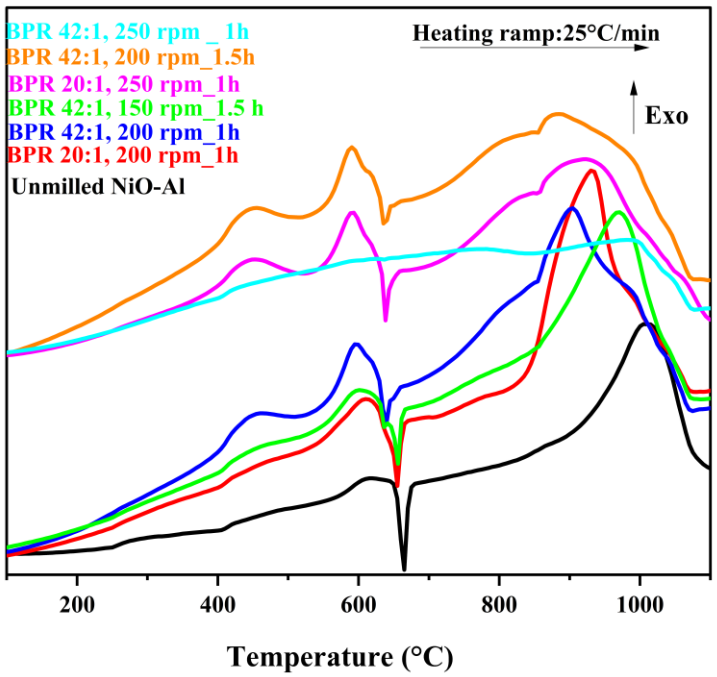

Figure 8. DSC plots comparing the unmilled NiO/Al mixture to the milled samples.

3.2. *Sintering process*

3.2.1 XRD analysis

The sintering process was applied to samples, wherein the final product was not formed using MA. Depending on the starting conditions applied to the NiO/Al system, the reduction process might occur during milling or sintering [39]. The milled samples sintered at 800 °C for 2 h were analysed using XRD, and the results are depicted in Figure 9. As observed, new phases of Ni and Al_2O_3 were formed during sintering, and the NiO peaks remained. This can be attributed to the low sintering temperature that is insufficient to ensure a complete reduction (800 °C < 904 and 930 °C) according to the present DSC results. Moreover, the quantity of NiO present in the pellet was not completely reduced. However, we observed a marginal reduction in the intensity of the peaks as the peak corresponding to the sample milled with a BPR of 42:1 broadened wider than that milled with a BPR of 20:1. The XRD profile of the milled sample sintered at 1100 °C for 2 h is portrayed in Figure 10. Moreover, the sharp intense peaks were recorded for both Ni and Al_2O_3 phases; the presence of NiO in the mixture after sintering likely resulted from the oxygen present within the tube during the sintering process. Additionally, it may be associated with the oxidation of nickel during the extraction of the mixture following the milling process. As the analytical section presided over molten Al_2O_3, alumina peaks were more frequent than nickel peaks. A similar tendency was observed in the X-ray study performed by Jones et al. [40].

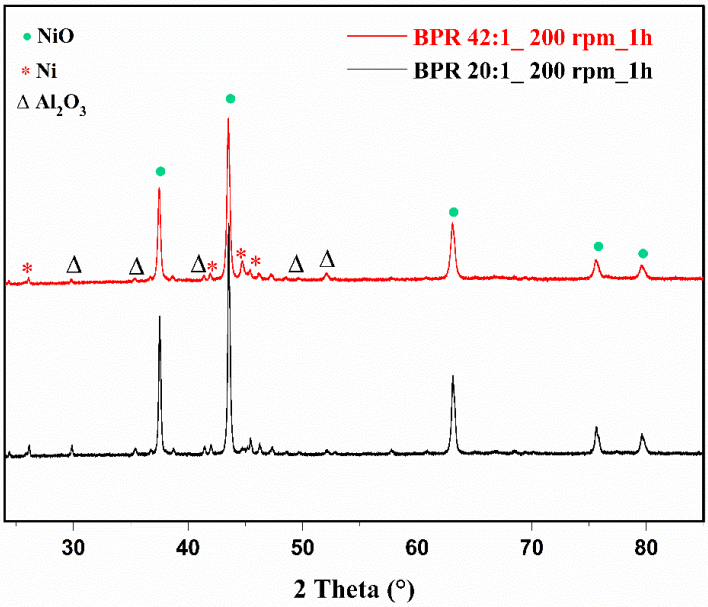

Figure 9. XRD patterns of milled and sintered samples at 800°C for 2 hours.

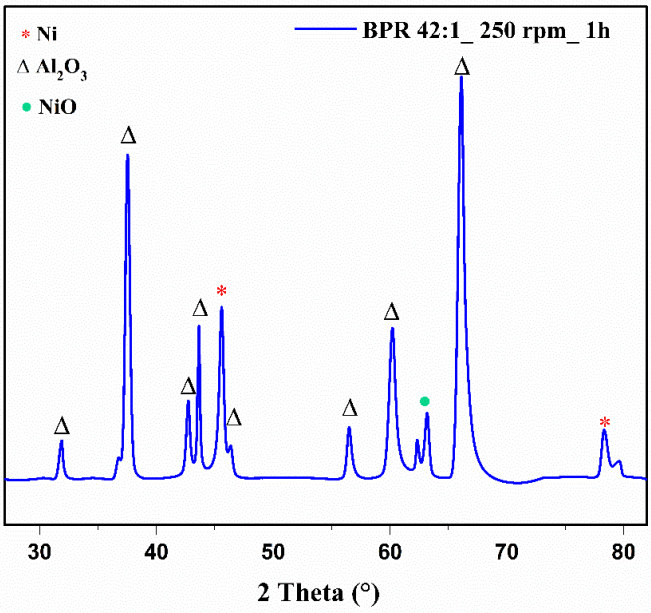

Figure 10. XRD profile of milled and sintered sample at 1100°C for 2 hours.

3.2.2. SEM microstructure

The morphology of the new product phases in the samples sintered at 800 °C for 2 h is depicted in Figure 11. As observed in Figure 11(a) and (c), the product particles were arranged in a homogenous distribution with no agglomeration. The number of voids in the composite is reflected in the dark zones; dark grey particles denote Al_2O_3, whereas white particles represent the Ni phase. The EDS analysis of both the sintered samples revealed no contamination during milling or/and sintering; only the reactants and product elements were detected. The composition of the area in Figure 11(b) was nearly identical to that in (d). Despite selecting an extremely small area of analysis, all the selected areas did not exhibit a single phase, depicting fine grains and particles of the composite. In the sintering process, the thermal conditions applied to compacted powder particles promote grain growth, allowing them to connect to each other across of grain boundaries. Increasing the sintering temperature promotes increased grain growth, resulting in a reduction of the trapped air between particles and subsequently enhancing the density of the samples[33]. The microstructure of the specimen milled with a BPR of 42:1, speed of 250 rpm for 1 h, and sintered at 1100 °C for 2 h is depicted in Figure 12. After sintering, the recovered sample was melted in a ceramic container, where it nearly separated into two parts—nickel and alumina. The mapping analysis in the Ni phase (Figure 12(a)) exhibited the presence of oxygen and Al, but with low concentrations. Similar observations were recorded for mapping the alumina phase, and the amount of nickel was considerably small (Figure 12(b)).

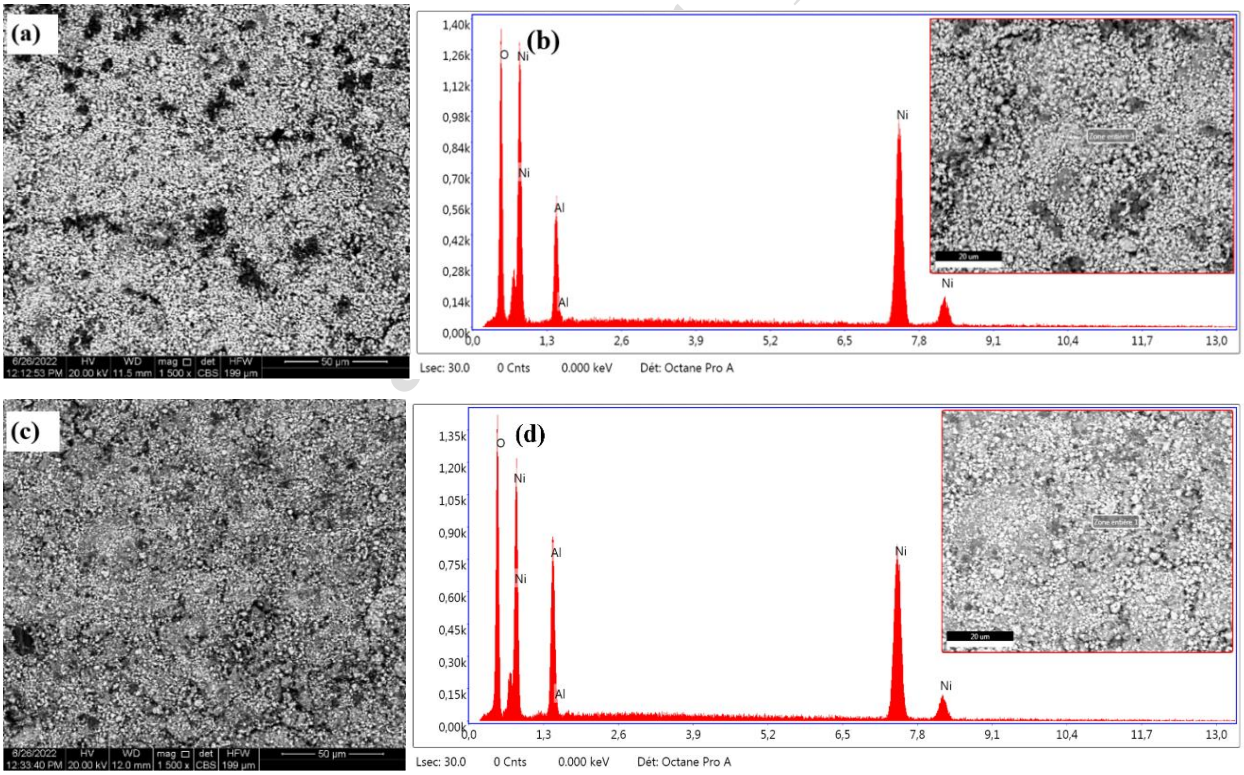

Figure 11. SEM images and EDS plots of sintered samples at 800°C for 2 hours of (a, b) BPR 20:1 and 200 rpm for 1hour, (c, d) BPR 42:1 and 200 rpm for 1 hour.

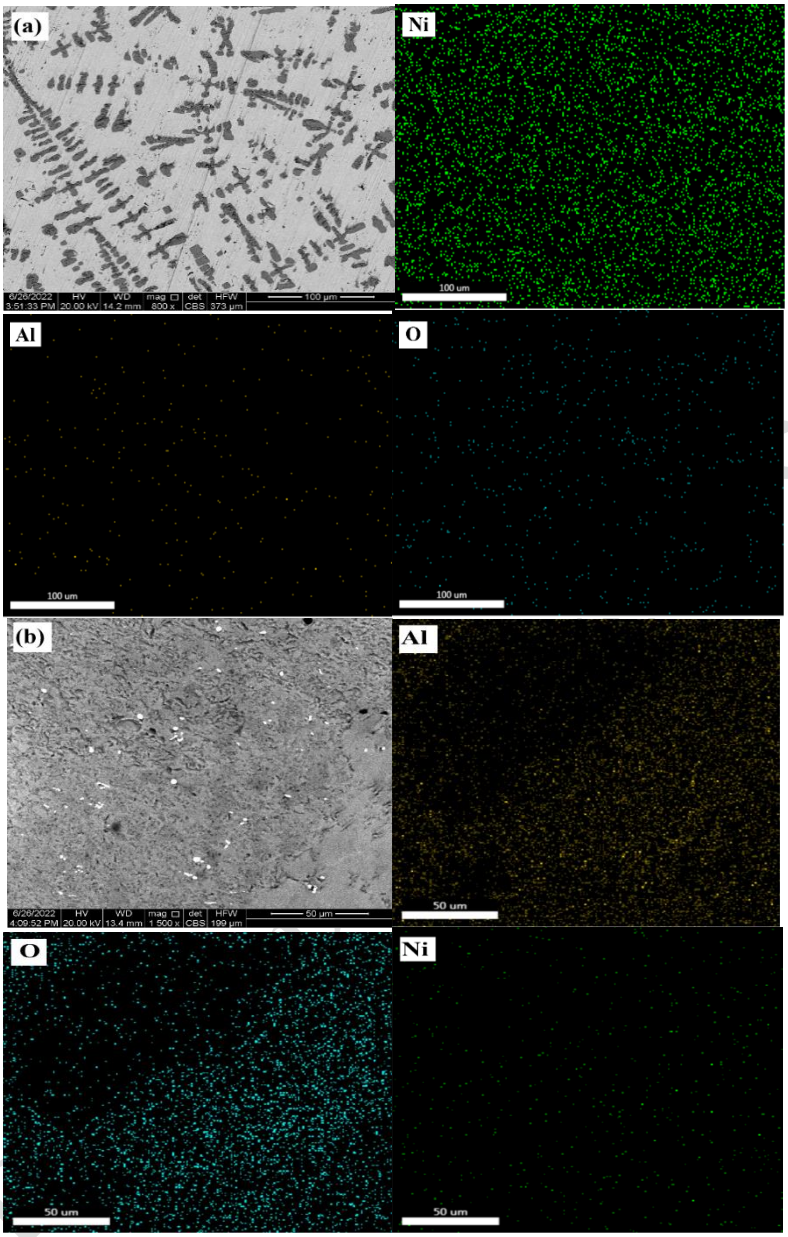

Figure 12. SEM images and EDS mapping of sintered sample at 1100°C for 2 hours (a) Nickel phase and (b) Alumina phase.

3.3 Tribological Properties

3.3.1 Effect of milling and the applied load on the friction coefficient

Milling parameters wield a significant and consequential influence upon both the microstructural properties of the acquired powder mixtures and the resulting sintered composites, as a result, they have a significant influence on their respective tribological properties. Two samples were examined: (a) an unmilled sample sintered at 1100°C and (b) a sample milled with a BPR of 42:1 at 200 rpm for 1 hour and subsequently sintered at 1100°C. The tests were conducted under standard environmental conditions, subjecting the specimens to vertical forces of 5 N and 10 N, with a sliding distance of 50 m and a sliding speed of 25 mm/s. Figure 13 depicts the development

of the friction coefficient for both samples. It is noticeable that as the applied load increases, the friction coefficient increases in both samples. Increasing the applied load from 5 to 10 N increases the friction coefficient of the unmilled sample from 0.48 to 0.66, respectively. Moreover, the friction coefficients of milled sample reached 0.44 and 0.60 when applying loads of 5 and 10 N, respectively. An increase in the friction coefficient may occur as a result of the removal of surface asperities, which leads to the formation of a third body. These particles from the third body, located at the contact surface, contribute to elevated value of friction [40- 42]. It's worthwhile to notice that the coefficient of friction reduces with milling. These findings show the impact of milling on the friction coefficient. The decreased coefficient of friction observed in milled sample can be attributed to the occurrence of work hardening resulting from the repeated fracture and welding caused by milling. As a result, the Young's modulus increased, leading to a reduction in the friction coefficient[43].

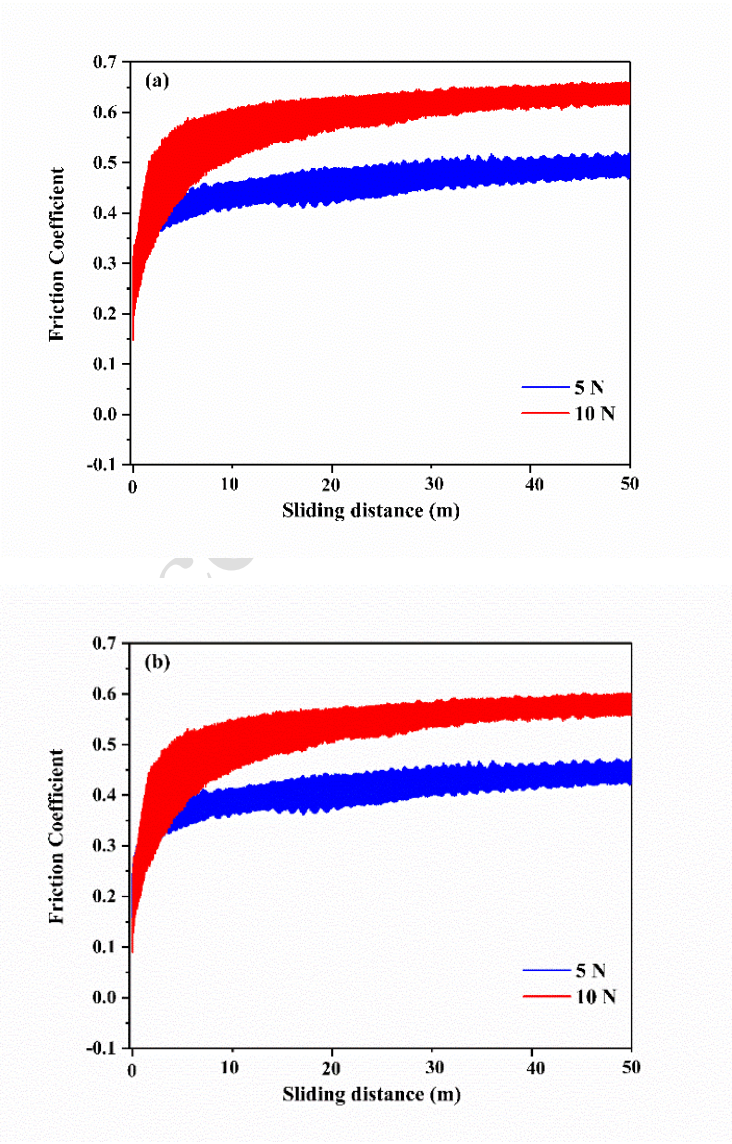

Figure 13. Impact of applied forces (5 and 10 N) on the friction coefficient of sintered specimens, (a) unmilled sample and (b) a sample milled with a BPR of 42:1 at 200 rpm for 1 hour and subsequently sintered at 1100°C

3.3.2 Wear mechanism

Figure 14 reveals the worm surface of the two sintered specimens (a) unmilled (10N) and (b) milled with a BPR of 42:1 at 200 rpm for 1 hour (5 and 10 N). As observed, Figure 14 (a) the worn surface displays clear signs of abrasive wear, featuring the emergence of several micro-cracks. Due to the existence of micro-cracks, particles can be readily dislodged from the matrix, resulting in the creation of a rough wear track. The primary factor contributing to the significant weight loss is the detachment of particles. As depicted in Figure 14b (SEM), the wear tracks on the specimens subjected to a 10 N load are characterized by their depth and narrowness, in contrast to those exposed to 5 N loads. A minimal quantity of debris was detected around the wear track. Moreover, the worn surfaces of sample (b) reveals the presence of plastic deformation and more cracks. An extensive examination of changes in the 3D surface morphology of both sintered samples with an applied load of 10N was provided in figures 14 (c and d). The mean wear track depth measured -18 µm for milled and sintered specimens compared to -5 µm for the unmilled samples. The irregularities observed at the base of the wear tracks, particularly as shown in Figure 14(d), suggest that abrasive wear is also a common occurrence during contact. This is likely attributed to three-body abrasion mechanisms resulting from the fragmentation of oxide particles and wear debris[44]. The findings above suggest that the tribological characteristics are influenced by operational factors such as applied loads and the chemical composition which as mentioned in the first part depends on milling parameters. Milling has a major impact on the grain size and phases formed, which helps explain why the friction coefficient and worm surfaces of samples milled was different from the unmilled.

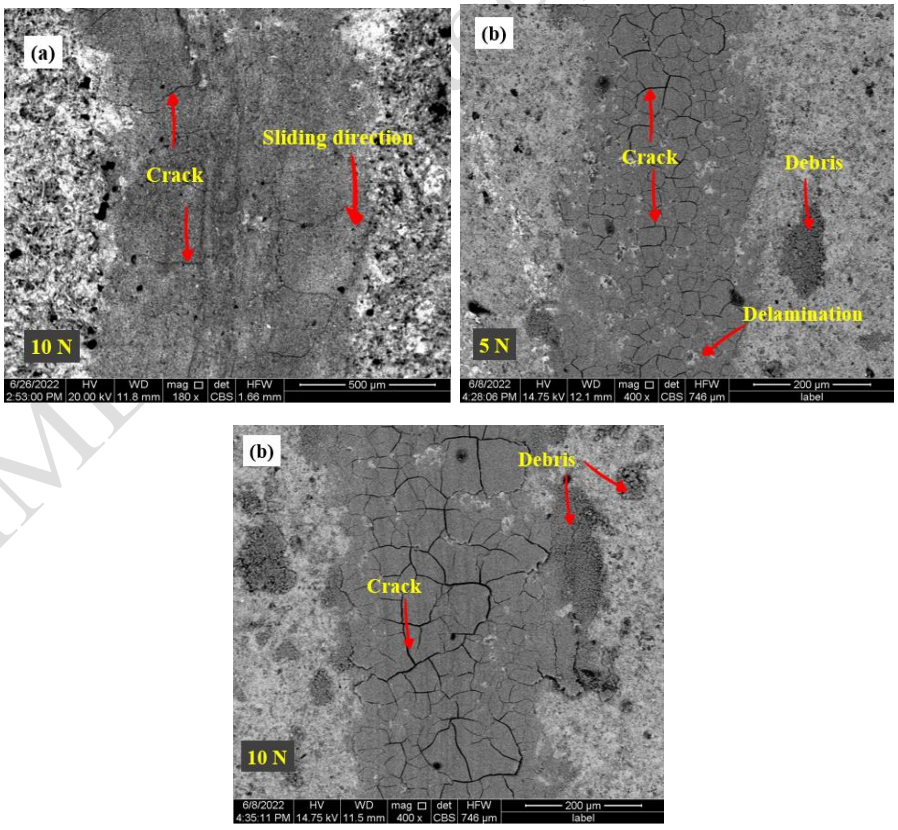

JMMP Accepted Manuscript

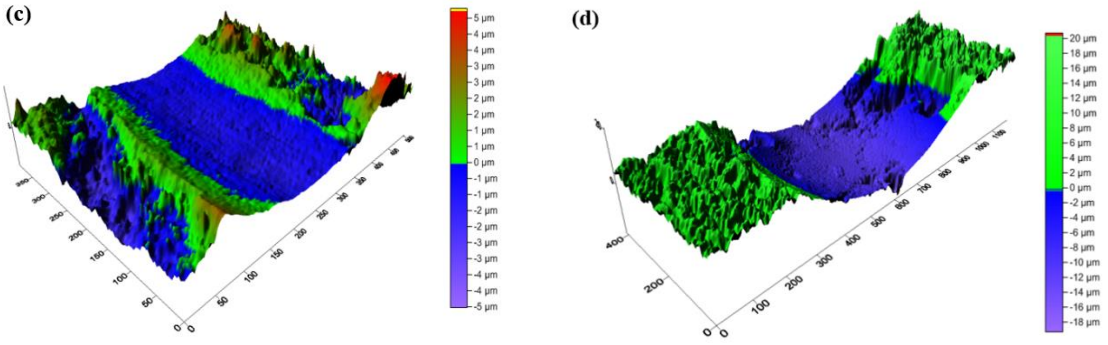

Figure 14. SEM images and 3D morphologies of worm surfaces (a) *unmilled (10N) , (b) milled with a BPR of 42:1 at 200 rpm for 1 hour (5 and 10 N),(c)3D of the unmilled sample at 10N and (d) 3D milled sample at 10 N.*

4. Conclusions

This study successfully investigated the synthesis, characterization and tribological performance of Ni/Al_2O_3 nanocomposites obtained by mechanical alloying. In particular, we examined the effect of milling parameters on the refinement of reactant (NiO and Al) powders and production of Ni/Al_2O_3 nanocomposite without adding PCAs. Sintering process has been used to densify the milled powder mixtures. The inferences derived from the present findings are summarised as follows:

- Increasing the BPR from 20:1 to 42:1 improved the particle refinement of the reactants and products for each applied speed (100, 150, 200, and 250 rpm). Moreover, homogenous powders at a nanometre-scale were obtained upon exploring the effect of prolonged milling duration with a low milling speed; no composite or intermetallic was detected even after milling for 8 h.
- In case of a BPR of 42:1 with a speed of 200 rpm for 1.5 h, we could generate Ni/Al_2O_3 nanocomposites with particle sizes of 85 nm for Ni particles and 45 nm for alumina.
- The findings of SEM and EDS revealed the formation of the metallic matrix nanocomposite *via* the mechanochemical interaction between NiO and Al and confirmed the crystallite size calculations using the W–H plot.
- The DSC data of the milled samples revealed that uncompleted milling reactions might occur during sintering at lower temperatures than those in the unmilled sample.
- The XRD patterns of the samples sintered at 800 °C for 2 h exhibited peaks of Ni and alumina phases with traces of unreduced NiO. In particular, the thermite reactions reduced the unreacted NiO and Al during sintering at 1100 °C for 2 h.
- The friction coefficient increases with applied forces and decreases with milling.
- SEM and 3D morphologies of the worn surface clearly showed that abrasion was the predominant wear process.

Acknowledgements

The High Resolution Powder Diffraction experiments were performed at the European Synchrotron Radiation Facility (Grenoble, France) on beamline ID31. The authors would like to express their particular gratitude to Andy Fitch for the beamtime and experimental assistance.

JMMP accepted manuscript

Author contribution

Nor El-Houda Berramdan (PhD student): conceptualization, experimental work, investigation, resources, writing - original draft, writing - review and editing, and visualisation. Hafida Boutefnouchet (supervisor): methodology, resources, review and editing. Mosbah Zidani: supervision, visualization and validation. Ridvan Yamanoglu: technical support and help with characterisation. Caroline Curfs: technical support and help with characterisation.

Data availability

Not applicable.

Conflict of interest

The authors declare no competing interests.

Journal pre-accepted manuscript

References

[1] C. Suryanarayana, "Mechanical Alloying: A Novel Technique to Synthesize Advanced Materials," *Research*, vol. 2019, pp. 1–17, 2019, doi: 10.34133/2019/4219812.

[2] L. Takacs, "Self-sustaining reactions induced by ball milling," *Prog. Mater. Sci.*, vol. 47, no. 4, pp. 355–414, 2002, doi: 10.1016/S0079-6425(01)00002-0.

[3] W. Xia and M. Zarezadeh, "Direct synthesis of NiAl intermetallic matrix composite with TiC and Al 2 O 3 reinforcements by mechanical alloying of NiO – Al – Ti – C powder mixture," *Ceram. Int.*, vol. 47, no. 19, pp. 26863–26868, 2021, doi: 10.1016/j.ceramint.2021.06.095.

[4] S. Arasteh, A. Masoudi, A. Abbasi, and S. Lotfian, "Mechanical Activation-Assisted Solid-State Aluminothermic Reduction of CuO Powders for In-Situ Copper Matrix Composite Fabrication," *Metals (Basel).*, vol. 12, no. 8, 2022, doi: 10.3390/met12081292.

[5] A. Maleki, N. Hosseini, and B. Niroumand, "Review article A review on aluminothermic reaction of Al / ZnO system," *Ceram. Int.*, no. June, pp. 0–1, 2017, doi: 10.1016/j.ceramint.2017.09.168.

[6] C. Alekhya, A. Prajoshna, M. Ayaz Baig, C. Chandrika, A. Devaraju, and S. Gadakary, "Preparation and characterization of Al-TiO2-Mg composites through powder metallurgy," *Mater. Today Proc.*, vol. 66, pp. 489–495, 2022, doi: 10.1016/j.matpr.2022.03.725.

[7] P. M. Botta, R. C. Mercader, E. F. Aglietti, and J. M. Porto López, "Synthesis of Fe-FeAl2O4-Al2O3 by high-energy ball milling of Al-Fe3O4 mixtures," *Scr. Mater.*, vol. 48, no. 8, pp. 1093–1098, 2003, doi: 10.1016/S1359-6462(02)00630-9.

[8] L. Chen, J. Yang, Y. Yang, Y. Zhang, and Z. Wang, "Thermodynamics, kinetics and mechanism analysis of aluminothermic reduction for preparing Al-Zr alloy," *Mater. Today Commun.*, vol. 31, no. May, p. 103714, 2022, doi: 10.1016/j.mtcomm.2022.103714.

[9] A. S. Mukasyan, A. S. Rogachev, and S. T. Aruna, "Combustion synthesis in nanostructured reactive systems," *Adv. Powder Technol.*, vol. 26, no. 3, pp. 954–976, 2015, doi: 10.1016/j.apt.2015.03.013.

[10] R. Ebrahimi-Kahrizsangi, M. Abdellahi, and M. Bahmanpour, "Ignition time of nanopowders during milling: A novel simulation," *Powder Technol.*, vol. 272, pp. 224–234, 2015, doi: 10.1016/j.powtec.2014.12.009.

[11] A. Yazdani and T. Isfahani, "Hardness, wear resistance and bonding strength of nano structured functionally graded Ni-Al2O3 composite coatings fabricated by ball milling method," *Adv. Powder Technol.*, vol. 29, no. 5, pp. 1306–1316, 2018, doi: 10.1016/j.apt.2018.02.025.

[12] A. YAZDANI and T. ISFAHANI, "A facile method for fabrication of nano-structured Ni-Al2O3 graded coatings: Structural characterization," *Trans. Nonferrous Met. Soc. China (English Ed.*, vol. 28, no. 1, pp. 77–87, 2018, doi: 10.1016/S1003-6326(18)64640-0.

[13] D. Vrel, A. Hendaoui, P. Langlois, S. Dubois, V. Gauthier, and B. Cochepin, "SHS reactions in the NiO-Al system: Influence of stoichiometry," *Int. J. Self-Propagating High-Temperature Synth.*, vol. 16, no. 2, pp. 62–69, 2007, doi: 10.3103/s1061386207020021.

[14] D. Vrel, P. Langlois, E. M. Heian, N. Karnatak, S. Dubois, and M. F. Beaufort, "Reaction Kinetics and Phase Segregation in the 3NiO+ 2Al 3Ni+ Al2O3 Thermite System," *Int. J. SHS*, vol. 12, no. 4, pp. 261–270, 2003.

[15] R. Troncy, G. Bonnet, F. Pedraza, and L. R. Universit, "Microstructural characterization of NiAl – Al 2 O 3 composite materials obtained by in situ aluminothermic reduction of NiO for potential coating applications," *Mater. Chem. Phys.*, vol. 251, no. April, p. 123124, 2020, doi: 10.1016/j.matchemphys.2020.123124.

[16] R. Troncy, G. Bonnet, and F. Pedraza, "Synthesis of self-regenerating NiAl-Al2O3 composite coatings," *Mater. Chem. Phys.*, vol. 279, no. March 2021, p. 125647, 2022, doi: 10.1016/j.matchemphys.2021.125647.

[17] M. Beyhaghi, J. Vahdati Khaki, M. Manawan, A. Kiani-Rashid, M. Kashefi, and S. Jonsson, "In-situ synthesis and characterization of nano-structured NiAl-Al2O3 composite during high energy ball milling," *Powder Technol.*, vol. 329, pp. 95–106, 2018, doi: 10.1016/j.powtec.2018.01.052.
[18] A. Goudarzi, A. Lalianpour, M. Zarezadeh Mehrizi, R. Beygi, and G. Eisaabadi B, "Fabrication of NiAl–Al2O3-WC nanocomposite by mechanical alloying and subsequent heat treatment," *Ceram. Int.*, vol. 45, no. 15, pp. 19049–19054, 2019, doi: 10.1016/j.ceramint.2019.06.147.
[19] W. Gui, J. Lin, M. Liu, Y. Qu, Y. Wang, and Y. Liang, "Effects of nano-NiO addition on the microstructure and corrosion properties of high Nb-TiAl alloy," *J. Alloys Compd.*, vol. 782, pp. 973–980, 2019, doi: 10.1016/j.jallcom.2018.12.200.
[20] L. U. O. Fa, "Mechanical and dielectric properties of Ni / Al 2 O 3 composites," vol. 45, no. 50572090, pp. 662–665, 2007.
[21] Z. Adabavazeh, F. Karimzadeh, and M. H. Enayati, "Mechanochemical behavior of NiO-Al-Fe powder mixtures to produce (Ni, Fe)3Al-Al2O3 nanocomposite powder," *Metall. Mater. Trans. A Phys. Metall. Mater. Sci.*, vol. 43, no. 9, pp. 3359–3365, 2012, doi: 10.1007/s11661-012-1138-0.
[22] P. Matteazzi and G. Le Caër, "Synthesis of Nanocrystalline Alumina–Metal Composites by Room-Temperature Ball-Milling of Metal Oxides and Aluminum," *J. Am. Ceram. Soc.*, vol. 75, no. 10, pp. 2749–2755, 1992, doi: 10.1111/j.1151-2916.1992.tb05499.x.
[23] J. Li, F. Li, and K. Hu, "Preparation of Ni/Al2O3 nanocomposite powder by high-energy ball milling and subsequent heat treatment," *J. Mater. Process. Technol.*, vol. 147, no. 2, pp. 236–240, 2004, doi: 10.1016/j.jmatprotec.2003.12.022.
[24] V. Udhayabanu, N. Singh, and B. S. Murty, "Mechanical activation of aluminothermic reduction of NiO by high energy ball milling," vol. 497, pp. 142–146, 2010, doi: 10.1016/j.jallcom.2010.03.089.
[25] A. Mameri, I. Daoud, A. Rezzoug, S. Azem, and R. Yamanoglu, "Tribological properties of in situ oxide reinforced nickel matrix composites produced by pressure-assisted sintering," *Int. J. Adv. Manuf. Technol.*, pp. 3731–3740, 2022, doi: 10.1007/s00170-022-08998-4.
[26] G. K. Williamson and W. H. Hall, "X-ray line broadening from filed aluminium and wolfram," *Acta Metall.*, vol. 1, no. 1, pp. 22–31, 1953, doi: 10.1016/0001-6160(53)90006-6.
[27] C. Suryanarayana, T. Klassen, and E. Ivanov, "Synthesis of nanocomposites and amorphous alloys by mechanical alloying," *J. Mater. Sci.*, vol. 46, no. 19, pp. 6301–6315, 2011, doi: 10.1007/s10853-011-5287-0.
[28] C. Suryanarayana, "Mechanical alloying and milling," *Prog. Mater. Sci.*, vol. 46, no. 1–2, pp. 1–184, 2001, doi: 10.1016/S0079-6425(99)00010-9.
[29] S. Z. Anvari, F. Karimzadeh, and M. H. Enayati, "Synthesis and characterization of NiAl-Al2O3 nanocomposite powder by mechanical alloying," *J. Alloys Compd.*, vol. 477, no. 1–2, pp. 178–181, 2009, doi: 10.1016/j.jallcom.2008.10.043.
[30] Y. Song, Y. Zhu, D. Gao, J. Guo, and H. S. Kim, "Computer Simulation and Verification of Adiabatic Temperature and Apparent Activity Energy of the NiO/Al Aluminothermic System," *J. Korean Powder Metall. Inst.*, vol. 20, no. 5, pp. 332–337, 2013, doi: 10.4150/kpmi.2013.20.5.332.
[31] A. M. Padhan, P. Ravikumar, P. Saravanan, and P. Alagarsamy, "Enhanced magnetic properties of NiO powders by the mechanical activation of aluminothermic reduction of NiO prepared by a ball milling process," *J. Magn. Magn. Mater.*, vol. 418, pp. 253–259, Nov. 2016, doi: 10.1016/j.jmmm.2016.01.057.
[32] A. Wagih, A. Fathy, O. Elkady, and A. M. Kabeel, "Author ' s Accepted Manuscript," *Ceram. Int.*, 2018, doi: 10.1016/j.ceramint.2018.12.053.
[33] A. Khamaj, W. M. Farouk, W. M. Shewakh, A. M. I. Abu-Oqail, A. Wagih, and M. Abu-Okail, "Effect of lattice structure evolution on the thermal and mechanical properties of Cu–Al2O3/GNPs nanocomposites," *Ceram. Int.*, vol. 47, no. 12, pp. 16511–16520, 2021, doi: 10.1016/j.ceramint.2021.02.219.
[34] A. Wagih and M. Shaat, "The dependence of accumulative roll bonded copper mechanical properties on grain sub-division, stacking faults, and lattice strains," *Mater. Sci. Eng. A*, vol. 756, no. December 2018, pp. 190–197, 2019, doi: 10.1016/j.msea.2019.04.061.
[35] A. Jabbarnia and S. Heshmati-manesh, "Effect of milling time on crystallite size and morphology of nickel aluminde based composite powder prepared by mechanical assisted SHS route," *Adv. Mater. Res.*, vol. 83–86, pp. 940–944, 2010, doi: 10.4028/www.scientific.net/AMR.83-86.940.
[36] A. Mameri, S. Azem, and A. Bilek, "Synthesis of Metallic and Intermetallic Matrix Composites Reinforced by Alumina by Reaction in NiO / Al Mixtures," *Trans. Indian Inst. Met.*, no. Lec2 M, 2017, doi: 10.1007/s12666-017-1205-8.
[37] M. Beyhaghi, A. Kiani-Rashid, J. V. Khaki, M. Kashefi, and S. Jonsson, "Influences of mechanical activation and heating rate on reaction processes in combustion synthesis of NiAl-Al 2 O 3 composites," *Powder Technol.*, vol. 346, pp. 237–247, 2019, doi: 10.1016/j.powtec.2019.01.072.
[38] A. M. Padhan, M. Sathish, P. Saravanan, and A. Perumal, "Mechanical activation on aluminothermic reduction and magnetic propertiesof NiO powders," *J. Phys. D. Appl. Phys.*, vol. 50, no. 21, p. aa6cee, 2017, doi: 10.1088/1361-6463/aa6cee.
[39] J. B. Fogagnolo, E. M. J. A. Pallone, D. R. Martin, C. S. Kiminami, C. Bolfarini, and W. J. Botta, "Processing of Al matrix composites reinforced with Al-Ni compounds and Al2O3 by reactive milling and reactive sintering," *J. Alloys Compd.*, vol. 471, no. 1–2, pp. 448–452, 2009, doi: 10.1016/j.jallcom.2008.03.125.
[40] S. A. Jones and J. M. Burlitch, "In situ formation of composites of alumina with nickel and with nickel aluminide," *Mater. Lett.*, vol. 19, no. 5–6, pp. 233–235, 1994, doi: 10.1016/0167-577X(94)90162-7.

JMMB-Accepted manuscript

[41] E. Geuzens *et al.*, "Synthesis and mechanical and tribological characterization of alumina-yttria stabilized zirconia (YSZ) nanocomposites with YSZ synthesized by means of an aqueous solution-gel method or a hydrothermal route," *Ceram. Int.*, vol. 34, no. 5, pp. 1315–1325, 2008, doi: 10.1016/j.ceramint.2007.03.001.
[42] K. P. Plucknett, C. Jin, C. C. Onuoha, T. L. Stewart, and Z. Memarrashidi, *The sliding wear response of high-performance cermets*. 2019.
[43] M. Fellah *et al.*, "Investigating the effect of milling time on structural, mechanical and tribological properties of a nanostructured hiped alpha alumina for biomaterial applications," *Arab. J. Chem.*, vol. 16, no. 10, p. 105112, 2023, doi: 10.1016/j.arabjc.2023.105112.
[44] Y. Y. Avcu *et al.*, "Surface and Tribological Properties of Powder Metallurgical Cp-Ti Titanium Alloy Modified by Shot Peening," *Coatings*, vol. 13, no. 1, pp. 1–20, 2023, doi: 10.3390/coatings13010089.

JMMB _accepted _manuscript

List of Figures

JMMB _ accepted _ manuscript

List of Tables

JMMB _accepted_ manuscript